Contributions to Mineralogy and Petrology (2023) 178:59
https://doi.org/10.1007/s00410-023-02038-4

ORIGINAL PAPER

Zirconium/hafnium fractionation and rare earth element systematics in sub-cratonic garnet pyroxenites, Norway

Dirk Spengler[1,2] · **Joachim Opitz**[2]

Received: 6 September 2022 / Accepted: 17 July 2023

Abstract

Ten previously studied garnet pyroxenites and one eclogite from orogenic peridotites in the Western Gneiss Region of Norway were analysed for whole-rock major and trace and mineral trace elements to characterise the evolutionary stages of the East Greenland sub-cratonic mantle. A continuous range of whole-rock MgO contents (17–30 wt.%) correlates inversely with Na_2O, Al_2O_3, and CaO contents. In contrast, rare earth element (REE) compositions allow the samples to be devided into two types. Type I samples have relatively flat primitive mantle (PM) normalised REE patterns (0.4−6.8 times PM values) with minor fractionation of middle–heavy REEs. Type II samples are simlar to type I samples but have higher light REE contents (6.1–57 times PM values) that reflect metasomatic enrichment. Whole-rock Zr contents (1–27 µg g^{-1}) and Zr/Hf ratios (17–39) are positively correlated. Type I samples have low Zr/Hf ratios that mostly differ from type II samples, indicating that metasomatism modified the initially sub-chondritic Zr/Hf ratios. Garnet Zr–Zr/Hf–Y–Ti systematics suggest that metasomatic enrichment transformed the type I samples into type II samples, consistent with processes observed in other cratonic areas (e.g., the northern East European Platform and the Kaapvaal Craton). The formation of type I pyroxenite in dunite from a melt at ~ 100 km depth implies the sub-chondritic Zr/Hf ratios were inherited from that melt. Such melts are thought to form by melting of garnet-bearing, melt-depleted mantle, which is consistent with models for recycling of Archaean palaeo-oceanic crust throughout the mantle prior to the formation of the sub-cratonic lithosphere beneath East Greenland.

Keywords Archaean lithospheric mantle · Garnet pyroxenite · REE · Western Gneiss Region · Zr/Hf fractionation

Introduction

Extensive mantle melt depletion has been experimentally shown to form chemically infertile, residual mantle lithologies (Walter 1998). The subcontinental lithospheric mantle (SCLM) beneath cratons worldwide contains such residual lithologies (i.e. harzburgite and dunite). These rocks usually lack the two major host minerals for incompatible elements in the upper mantle (garnet and clinopyroxene), and these two minerals can also record the physical conditions during melt extraction (Herzberg 2004; Pearson and Wittig 2008). Once garnet and clinopyroxene are exhausted during mantle melting, information regarding the melting conditions is largely inaccessible, and the residue becomes susceptible to secondary chemical overprints, which can re-form these minerals in the melt-depleted rocks and further obscure their earlier history (Griffin et al. 2003). However, the details of the initial melting conditions are key to reconstructing the geodynamic processes that formed sub-cratonic mantle and, in particular, Archaean SCLM.

Garnet pyroxenite and eclogite are minor components in the harzburgites and dunites of the East Greenland SCLM that were tectonically transported to western Norway (Brueckner 1998; Beyer et al. 2006, 2012; Spengler 2006). These minor lithologies contain incompatible elements that have been added to the melt-depleted peridotites during one or several Proterozoic re-fertilisation events (Brueckner et al. 2002; Beyer et al. 2006; Cutts et al. 2019). In the case of the East Greenland SCLM, re-fertilisation occurred

Communicated by Daniela Rubatto.

✉ Dirk Spengler
dirk@spengler.eu

[1] Faculty of Geology, Geophysics and Environmental Protection, AGH University of Science and Technology, 30-059 Krakow, Poland

[2] Institute of Mineralogy and Crystal Chemistry (closed), University of Stuttgart, Azenbergstraße 18, 70174 Stuttgart, Germany

Published online: 10 August 2023

long after the Archaean melt depletion event that has been dated with t_{MA} ages (these are maximum ages and assume all measured Re was present since the melt extraction) of 2.7–3.4 Ga using Re–Os isotope data from olivine and orthopyroxene mineral separates and whole-rocks of the dunites (Beyer et al. 2004; Spengler 2006). However, Sm–Nd and Lu–Hf isotope data for garnet and garnet pyroxenite whole-rocks also show that fertile components have an Archaean age (Jamtveit et al. 1991; Spengler et al. 2006, 2009; Cutts et al. 2019), as do sulphides in a garnet orthopyroxenite (Brueckner et al. 2002). The oldest radiogenic isotope ages obtained from the fertile lithologies of 3.1–3.3 Ga (Re–Os and Sm–Nd isotope data) overlap with the age of the melt depletion event during the mid-Archaean (Re–Os isotope data). This indicates that two evolutionary stages—melting and refertilisation—occurred within the temporal resolution of the geochronological methods. This study used major and trace element data for the fertile components to constrain the nature of the re-fertilisation event.

Geological setting and sample locations

The early Palaeozoic convergence of Laurentia and Baltica closed the Iapetus Ocean and formed a series of thrust nappes on the plate margin of Baltica (Gee et al. 2013) known as the Scandinavian Caledonides. The Western Gneiss Region (WGR) in Norway represents a tectonic window through these nappes into the lowermost tectono-stratigraphic unit. The exposed rocks are dominated by high-grade quartzo-feldspathic gneisses with Proterozoic protolith ages (Tucker et al. 1990) that were reworked during the Caledonian Orogeny (Kullerud et al. 1986). Together with the infolded supracrustal rocks, this lowermost unit is thought to represent the western margin of Baltica. The gneisses are dominated by amphibolite- and granulite-facies mineralogies and contain numerous mafic rock bodies with a (partially retrogressed) eclogite-facies mineralogy (Griffin et al. 1985). Nearly 20 Mg–Cr garnet peridotite bodies occur throughout the WGR (Fig. 1a). These ultramafic rocks have geochemical characteristics that are consistent with the SCLM (Carswell et al. 1983), with a Laurentian provenance (Beyer et al. 2012).

The peridotites are compositionally layered; individual layers vary in composition between dunite, harzburgite, garnet-dunite, garnet-harzburgite, and minor garnet-lherzolite. Magnesian olivine (forsterite 92–95) suggests that dunite experienced high degrees of melt extraction of 50% to > 60% (Carswell et al. 1983; Beyer et al. 2006; Spengler 2006). Layers (and minor lenses) of garnet pyroxenite occur parallel to the peridotite compositional layering (Fig. 1b). Detailed petrography and whole-rock chemistry of peridotite and garnet pyroxenite suggest that mechanical mixing of both rock types formed the mineralogical layering, in peridotite exposed in the WGR and the opposite site of the orogen (Brueckner 2018; Spengler et al. 2018). All garnet-bearing mantle lithologies in the WGR contain oriented mineral microstructures that formed after majoritic garnet (van Roermund and Drury 1998; Spengler et al. 2006). The origin of these fertile components (i.e., garnet pyroxenite and garnet that became mechanically mixed into peridotite) is considered to relate

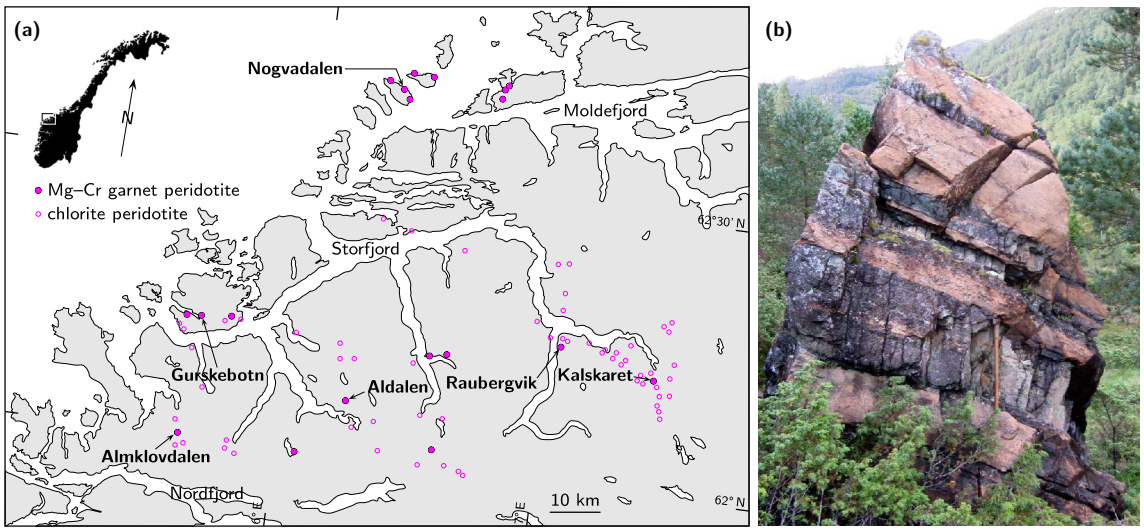

Fig. 1 Orogenic peridotites in the Western Gneiss Region of Norway. **a** Map showing the locations of the different types of peridotite bodies (adapted from Brueckner 2018) and sample locations (labelled). **b** Outcrop at Rødhaugen (Almklovdalen) containing a sharp contact relationship between dunite (light brown) and enclosed layers of garnet pyroxenite (dark colour). The hammer for scale = 80 cm in length (photograph: Franziska Scheffler)

to high-temperature mantle melts (Carswell 1973; Spengler et al. 2018).

The garnet peridotite bodies are proposed to have intruded the gneisses during the Caledonian subduction of Baltica beneath Laurentia (Brueckner 1998). Concomitant prograde metamorphism of the Baltica plate margin is indicated by the presence of corona-textured metadolerite and -gabbro (Griffin and Råheim 1973; Krabbendam et al. 2000) and mineral chemical zoning in the gneiss-hosted eclogites (Wain et al. 2000) and peridotite-hosted garnet pyroxenites (Fig. 1b; Spengler et al. 2019, 2021). The peak metamorphic conditions exceeded the graphite–diamond phase transition, as indicated by the presence of diamond in the gneisses (Dobrzhinetskaya et al. 1995), *in situ* diamonds in a crustal eclogite (Smith and Godard 2013), geothermobarometric data for crustal eclogites (Cuthbert et al. 2000), and geothermobarometric data for mantle pyroxenite minerals with Scandian (Caledonian) radiogenic isotopic ages (Spengler et al. 2009). Palaeogeographic reconstructions have determined that the source area of the ultramafic rocks was located at 69° N (present-day coordinates) in central East Greenland prior to Caledonian tectonism (Cocks and Torsvik 2005). At *ca*. 60 Ma, this area experienced lithospheric delamination and modification related to the passage of Greenland over the Iceland mantle plume (Steinberger et al. 2019).

All samples investigated in this study have been previously petrographically and petrologically characterised (Table SI-1). Nine garnet websterites and one garnet clinopyroxenite were investigated, and these were obtained from the garnet peridotite bodies at Almklovdalen (n = 3), Gurskebotn (n = 2), Kalskaret (n = 1), Nogvadalen (n = 2) and Raubergvik (n = 2). One additional mantle eclogite from the Aldalen body was also studied. In this study, we determined the whole-rock compositions of all garnet pyroxenites (n = 10). The mineral chemistry of the porphyroclasts was analysed in samples that lack intense recrystallisation (n = 9; Table SI-1). Each analysed grain contains oriented mineral inclusions, which are interpreted to have exsolved during cooling from high-temperature precursor minerals at high pressure (Spengler et al. 2021). One sample from Gurskebotn (DS1249) exhibits mineralogical layering that compositionally subdivides the hand-specimen into orthopyroxene-rich garnet websterite (DS1249a), orthopyroxene-poor garnet websterite (DS1249b), and garnet clinopyroxenite (DS1249c). The whole-rock composition of sample DS1249 was obtained on a ~ 1 cm thick rock slab, which includes all three compositional layers and may represent an average composition, whereas the mineral chemistry was obtained from each layer.

Methods

Whole-rock sample powders were produced after washing and crushing/powdering at the Institute of Geosciences, University of Potsdam, and the Institute of Mineralogy and Crystal Chemistry (IMK), University of Stuttgart, Germany. Each hand-specimen was wrapped in plastic and crushed using a hammer. The crushed fragments were aliquoted, and one aliquote was subsequently milled in an agate mortar. Powders weighing ~ 150 g were produced for each sample, except for samples AH0364 and FL99-26 (~ 100 g).

Fused glass discs were prepared at the IMK by mixing 0.6 g of sample powder with 3.6 g of $Li_2B_4O_7$ (BR A600 Specflux; Breitländer GmbH). A few milligrams of lithium-iodide were added at the end of the melting process to prevent the cooling glass from cracking. Whole-rock major element contents of the glass discs were determined by X-ray fluorescence (XRF) spectrometry using a PHILIPS PW 2400 instrument at the IMK. Certified geostandards were used for calibration.

The whole-rock trace element contents of the glass discs were determined using a 213 nm laser ablation (LA) system (Cetac LSX-213) coupled to an inductively coupled plasma mass spectrometer (ICP–MS; Agilent 7700) at the IMK. The ablation conditions were: beam diameter = 100–150 µm; laser energy = 35–100% of its maximum value (4 mJ at 150 µm); laser frequency = 10 Hz. Integration times were 22–24 s for the backgound and 29–37 s for the signal. The following isotopes were measured: ^{27}Al, ^{28,29}Si, ^{42,43,44}Ca, ^{45}Sc, ^{47,49}Ti, ^{51}V, ^{52}Cr, ^{55}Mn, ^{59}Co, ^{60}Ni, ^{85}Rb, ^{88}Sr, ^{89}Y, ^{90,91}Zr, ^{93}Nb, ^{133}Cs, ^{137}Ba, ^{139}La, ^{140}Ce, ^{141}Pr, ^{146}Nd, ^{147,149}Sm, ^{151,153}Eu, ^{157}Gd, ^{159}Tb, ^{161,163}Dy, ^{165}Ho, ^{166}Er, ^{169}Tm, ^{172}Yb, ^{175}Lu, ^{178}Hf, ^{181}Ta, ^{208}Pb, ^{232}Th, ^{238}U and ^{254}(^{238}U^{16}O). The relative elemental contents were obtained by external calibration using four reference materials (NIST SRM 610 and 612 glasses and DLH7 and DLH8 glasses from P&H Developments Limited). To obtain the absolute elemental contents, Si was used as an internal standard based on the contents measured by XRF spectrometry. The calibration procedures followed the protocols of Massonne et al. (2013). Whole-rock Zr/Hf ratios were measured using the same glass discs but under different analytical conditions. To achieve maximum sensitivity, the beam diameter was set to 150 µm, the laser energy to 80–100%, and the laser frequency to 10 Hz. Signals were recorded and processed off-line as described above. Only four isotopes were analysed: ^{90}Zr, ^{175}Lu, ^{178}Hf, and ^{181}Ta. Two calibrations were performed, one with all four reference glasses and another with two reference glasses (DLH7 and DLH8). The two Zr/Hf results per sample were subsequently averaged.

Mineral trace element contents were determined *in situ* along profiles across porphyroclastic grains in

150-µm-thick polished thin-sections using the previously described LA–ICP–MS system at the IMK. The sample surface was ablated with spots (beam diameter = 100 µm, laser energy = 40–100%, and laser frequency = 10 Hz). Integration times were 22–24 s for the backgound and 29–37 s for the signal. The ablated volume included uniformly distributed mineral inclusions (i.e., where present; typically in grain cores but not rims). Signals reflecting secondary elemental enrichments along cracks were excluded during the off-line data evaluation. Silica was used as an internal standard, with its elemental content being derived as a mean value from two individual results obtained from ^{28}Si and ^{29}Si and its absolute content being determined individually for each spot prior to LA using an electron microprobe at the IMK and the operating conditions described in Spengler et al. (2021). External calibration utilised the four aforementioned reference glasses. Reported average mineral compositions were only calculated from ablated mineral cores.

Results

Whole-rock major elements

The 10 garnet pyroxenite samples are magnesian in composition (MgO = 17.6−30.1wt.%; Table SI-2). The more melt-compatible elements have contents of Na_2O = 0.15 −0.92 wt.%, Al_2O_3 = 4.14−14.8 wt.%, and CaO = 6.28−13.7wt.%, which correlate negatively with MgO contents (Fig. 2). These features are indistinguishable from those of the other WGR garnet pyroxenites (Fig. 2). A major difference between the garnet clinopyroxenite and the garnet websterites is the higher TiO_2 content of the former (0.61 wt.% versus 0.03−0.50 wt.%, respectively).

Mineral trace elements

Trace element contents in garnet and clinopyroxene vary across the porphyroclastic grains and exhibit symmetrical or asymmetrical patterns (Fig. 3). Symmetrical patterns have shallow content gradients in grain cores and steep gradients in grain rims. In addition, oriented inclusions with a regular distribution occur either within whole grain cores or core domains but are absent in grain rims. Asymmetrical content patterns appear to be typical for samples that have experienced significant strain. The shallow elemental content gradients, as well as the presence of inclusions, can be used to recognise crystal core areas in asymmetrically eroded porphyroclasts. Only ablated spots from areas with shallow content gradients and inclusions (where present) were used to determine the average garnet and clinopyroxene compositions (Tables SI-3 and SI-4). Trace element contents of the porphyroclastic orthopyroxene were dominantly below the detection limits and are thus not reported.

Garnet

Garnet rare earth element (REE) contents allow the samples to be divided into two types. Type I garnet has low contents of light REEs, which are dominantly below detection limits (Fig. 4a). Contents of Gd–Lu exhibit minor to moderate fractionation and have 3–35 times the values of CI chondrite (McDonough and Sun 1995) that form normalised REE concentration patterns with positive slope. Contents of Zr include low values (0.6−11.2 µg g^{-1}), and the

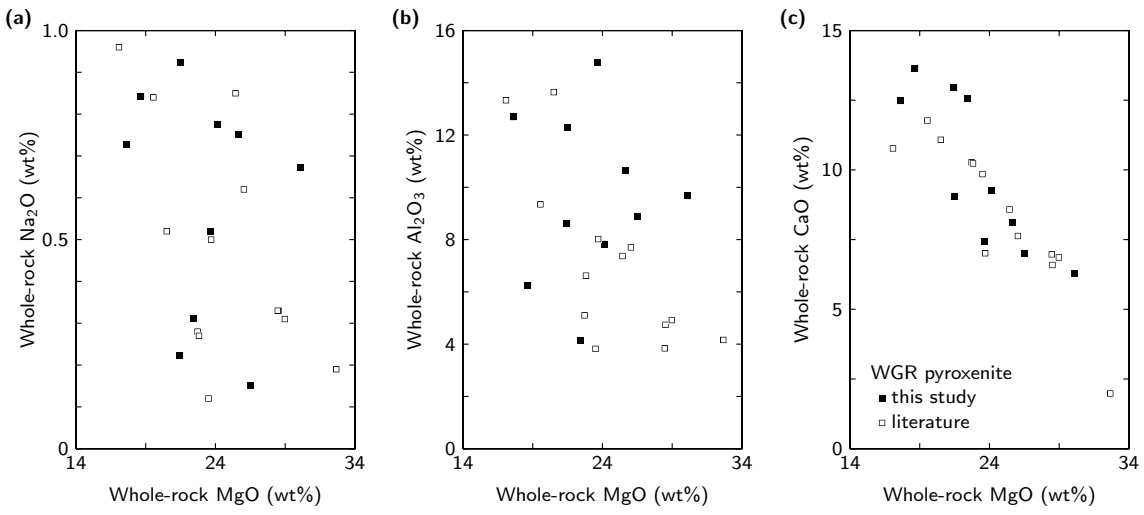

Fig. 2 Bivariate plots of whole-rock major element data for the Western Gneiss Region garnet pyroxenites analysed in this study (Table SI-2) and previous studies (Carswell 1973; Seljebotn 2016; Spengler et al. 2018)

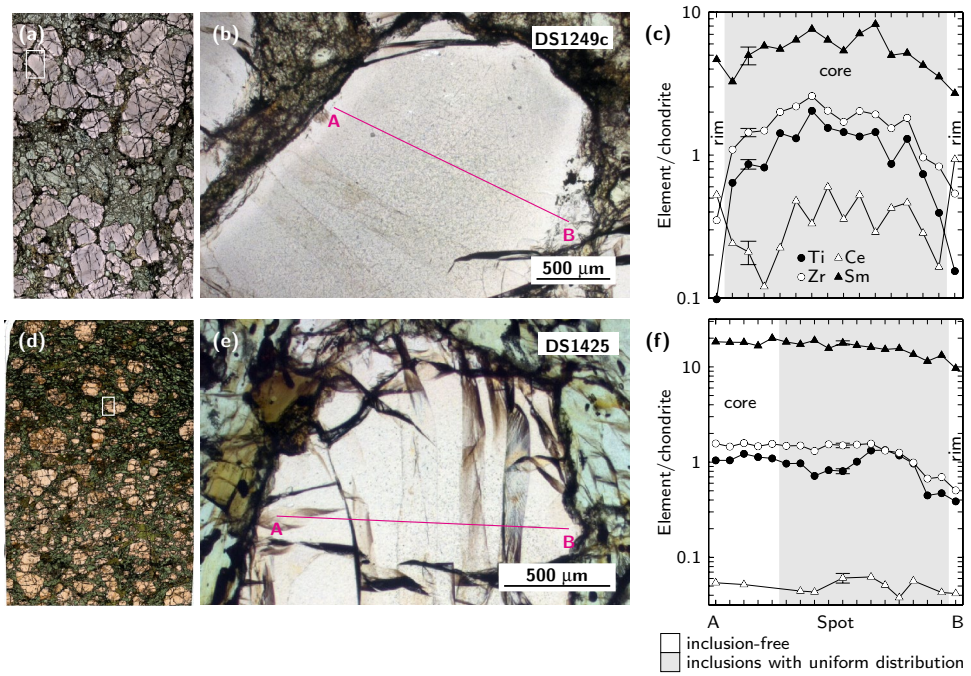

Fig. 3 Photomicrographs and selected trace element contents of garnet in two samples (**a–c** garnet websterite sample DS1249c; **d–f** eclogite sample DS1425). **a, d** Porphyroclastic grains of garnet (red) and clinopyroxene (bright green) associated with recrystallised garnet and clinopyroxene that is partially replaced by amphibole (dark green; scanned thin-sections; fields of view are 24 mm wide). Frames refer to the positions of the photomicrographs shown in **b** and **e**. **b, e** Porphyroclastic garnet (centre) containing uniformly distributed inclusions (mottled areas in grain interiors) and with inclusion-free rims (plane-polarised light). **c, f** LA–ICP–MS profiles (positions are indicated in **b** and **e**) showing elemental content gradients that are unrelated to the distribution of inclusions. Error bars show the standard error of the mean for selected spots. Normalisation values are from McDonough and Sun (1995)

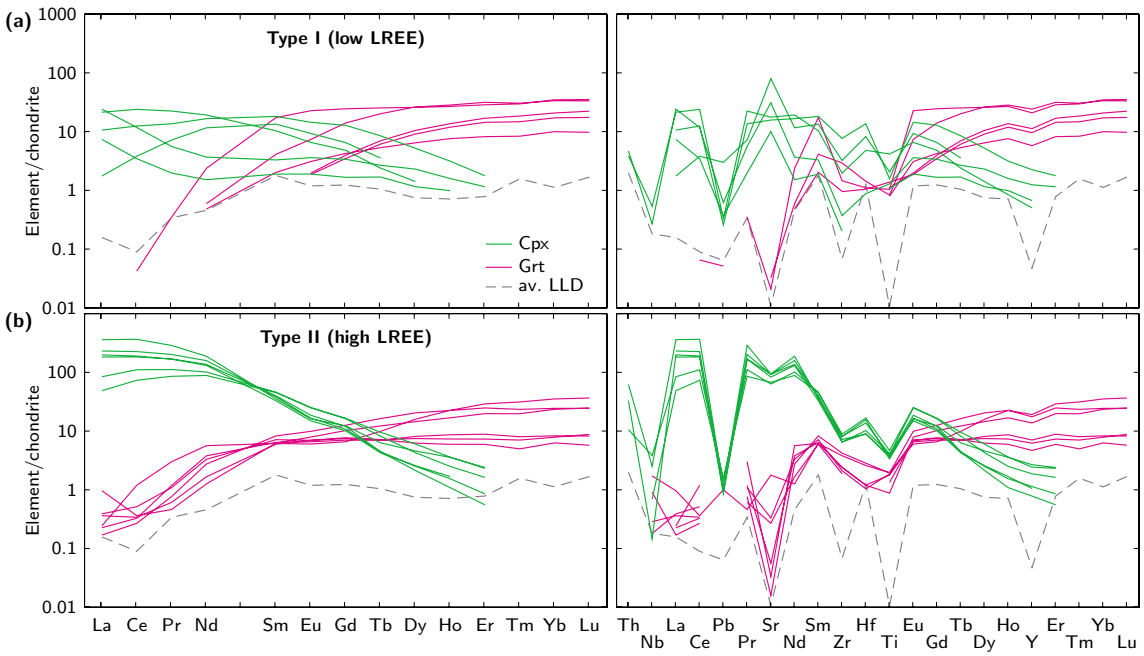

Fig. 4 Average trace element data for garnet (Grt) and clinopyroxene (Cpx) cores with uniformly distributed rutile ± pyroxene inclusions in the Western Gneiss Region pyroxenites and eclogite (left = REE data; right = multi-element data; Tables SI-3 and -4). Contents of mobile elements (light REEs, Sr) and Th divide the samples into two types. av. LLD = average lower limit of detection. Normalisation values are from McDonough and Sun (1995)

range narrows to 0.6–5.8 μg g^{-1} if sample DS0466 (Kalskaret) is excluded. Other elements with low contents are Hf (< 0.15 μg g^{-1}), Ti (350–608 μg g^{-1}), and Sr (< 0.25 μg g^{-1}). Yttrium (9–38 μg g^{-1}) defines a narrow compositional field when plotted versus Zr (Fig. 5a). The variable Zr contents do not correlate with Ti contents (Fig. 5b).

Type II garnet has high light REE contents that are above the detection limits (Fig. 4b). Contents of Gd–Lu exhibit minor to moderate fractionation, with 5–37 times chondritic values (i.e., similar to type I garnet). Contents of Zr are relatively high (7.2–16.1 μg g^{-1}). Other elements with high contents are Hf (0.11–0.29 μg g^{-1}), Ti (386–863 μg g^{-1}), and Sr (0.1–12.9 μg g^{-1}). Contents of Y (7–30 μg g^{-1}) are similar to those of type I garnet and form a separate, narrow compositional field in a plot versus Zr (Fig. 5a). The variable Zr contents correlate with Ti contents (Fig. 5b).

Clinopyroxene

The trace element chemistry of clinopyroxene also differs between the two types of samples (Fig. 4). Clinopyroxene in type I samples has low light REE contents that are 1.5–24 times chondritic values. Middle–heavy REEs form normalised concentration patterns with negative slope. Contents of Zr (0.8–29.2 μg g^{-1}) and Hf (< 0.1–1.4 μg g^{-1}) include low values and have wide ranges that exceed one order of magnitude. The range for Ti (474–1828 μg g^{-1}) narrows to 474–903 μg g^{-1} if sample DS0318 (Lien) is excluded. Contents of Sr (73–580 μg g^{-1}) and Th (< 0.04–0.14 μg g^{-1}) also include relatively low values and have wide ranges.

Type II clinopyroxene has high light REE contents that are 73–365 times chondritic values. Middle–heavy REEs form normalised concentration patterns with negative slope. Contents of Zr (24–34 μg g^{-1}) and Hf (0.9–1.7 μg g^{-1}) include high values and have narrow ranges, which is also the case for Ti (1478–2051 μg g^{-1}) and Sr (459–682 μg g^{-1}). The compositional range for Th (< 0.09–1.80 μg g^{-1}) also includes high values.

Whole-rock trace elements

The elemental contents that can be used to subdivide the mineral chemistry also apply to subdivision of the whole-rock chemistry (Table SI-5). Type I samples have relatively low contents of light REEs (0.4–6.8 times primitive mantle [PM] values; Fig. 6a). Contents of Gd–Lu indicate limited fractionation (0.8–3.9 times PM values). Contents of Zr have a wide range (1.1–17.3 μg g^{-1}) that narrows to 1.1–4.9 μg g^{-1} if sample DS0466 (Kalskaret) is excluded. Other elements have wide ranges and include low values: Hf = 0.04–0.74 μg g^{-1}, Ti = 223–3086 μg g^{-1}, Sr = 68–149 μg g^{-1}, and Th = 0.09–0.26 μg g^{-1}.

Type II samples have high light REE contents (6.1–57 times PM values), and contents of Gd–Lu exhibit minor fractionation (1.0–5.1 times PM values; Fig. 6b). Contents of Zr (13.7–16.4 μg g^{-1}), Hf (0.35–0.67 μg g^{-1}), Ti (1042–3723 μg g^{-1}), and Sr (141–235 μg g^{-1}) are relatively high and have narrow ranges. Contents of Th are mostly high (0.16–1.38 μg g^{-1}), unlike most of the type I samples.

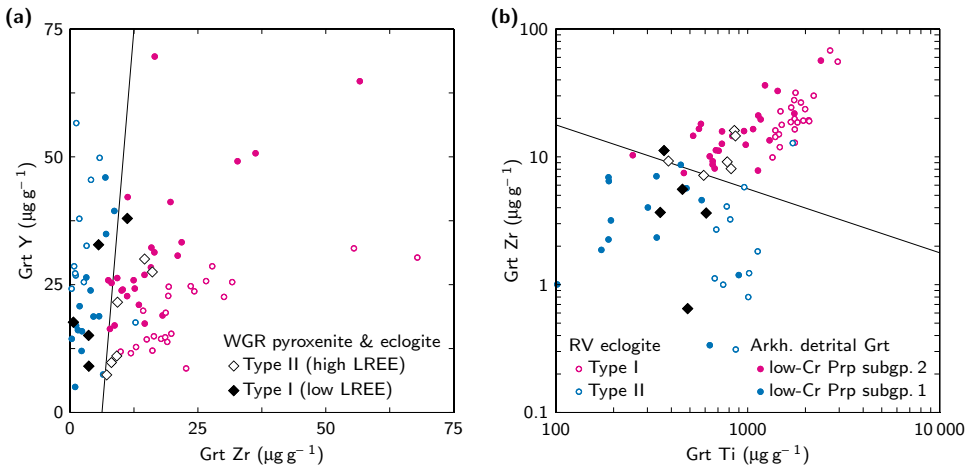

Fig. 5 Plots of trace element variations in garnet (Grt) from the Western Gneiss Region pyroxenites and eclogite. **a** Y versus Zr. **b** Zr versus Ti. Garnet in type I and II samples form clusters that overlap different types of garnet in the Roberts Victor (RV) eclogites (Gréau et al. 2011) and sub-groups of detrital low-Cr pyrope (Prp) with fractionated middle–heavy REEs in the Arkhangelsk alluvial sediments (Shchukina et al. 2019). Samples that record different degrees of metasomatic enrichment by a light REE-rich melt/fluid have minimal overlap and are separated by the annotated lines

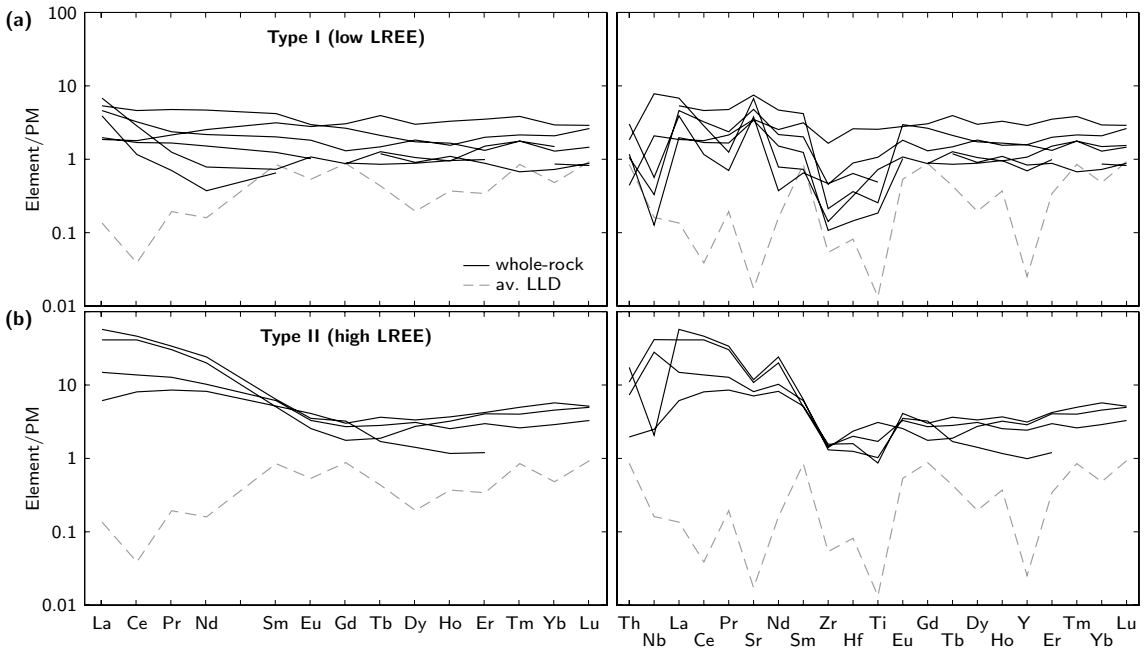

Fig. 6 Whole-rock trace element data for the Western Gneiss Region garnet pyroxenites, which are subdivided as in Fig. 4 (left = REE data; right = multi-element data; Table SI-5). av. LLD = average lower limit of detection (Table SI-7). Primitive mantle (PM) normalisation values are from McDonough and Sun (1995)

Discussion

Early history of the garnet pyroxenites and eclogite

The mantle samples exhibit scattered but continuous chemical trends in major elements (Fig. 2), suggesting they are genetically related. Limited whole-rock middle–heavy REE fractionation and content ranges of less than one order of magnitude (Fig. 6) are suggestive of a common origin for the entire sample suite. Because all the samples were derived from extremely melt-depleted harzburgite and dunite (Beyer et al. 2006; Spengler et al. 2006), their crystallisation environments were similar.

The equilibration depths of the studied garnet pyroxenites and eclogite in the SCLM are constrained by the mineral chemistry and oriented mineral inclusions in garnet to a narrow depth interval that corresponds to pressures of 3.4 ± 0.4 GPa (Spengler et al. 2021). A shallower depth of origin would not have allowed the formation of the exsolution microstructures of rutile and pyroxene in garnet (Fig. 2; Spengler et al. 2021), as observed in other samples from the same or adjacent peridotite bodies (van Roermund and Drury 1998; Terry et al. 1999; Spengler et al. 2009, 2019; Cuthbert and van Roermund 2010). As such, the studied samples had similar crystallisation depths.

Given that the studied samples have similar major element systematics (Fig. 2) and exhibits similarities in (1) contents and fractionation of less-mobile elements (e.g., heavy REEs), (2) mineral microstructures (Fig. 3), and (3) crystallisation environments (e.g., depth and host rock depletion), the timing of crystallisation is also expected to be similar. Sample Fl99-26 (Nogvadalen) yielded, together with nearby garnet pyroxenites, a Sm–Nd whole-rock isochron age of 3.33 ± 0.19 Ga (Spengler et al. 2009). This implies a mid-Archaean age for the sample. Other samples from the studied sample suite have not been analysed for radiogenic isotopes; however, other whole-rock garnet pyroxenites and garnets from the same and adjacent peridotite bodies have yielded Archaean radiogenic isotope ages, including Sm–Nd (Jamtveit et al. 1991; Spengler et al. 2006; Brueckner et al. 2010) and Lu–Hf (Cutts et al. 2019) ages. These differ from those determined by multi-mineral–whole-rock isochrons, which include a wide range of Proterozoic ages (Mearns 1986; Lapen et al. 2005; Brueckner et al. 2010; Cutts et al. 2019). A common age is thus assumed for most if not all of the studied samples; otherwise, an explanation is required as to why the mineral assemblages, mineral and whole-rock chemistries of less-mobile elements, and mineral microstructures are similar among the samples.

Metasomatism

Despite the similarities detailed above, the samples can be subdivided into types I and II (Figs. 4 and 6) based on their contents of more-mobile elements, such as light REEs, Th, and Sr (Gieré 1990; John et al. 2004; Tsay et al. 2017).

Enrichment of these elements in the type II samples suggests that metasomatism transformed type I samples into type II samples. This transformation modified the contents of Zr and Ti relative to Y, as is evident from the garnet chemistry (Fig. 5). Similar transformations as a result of metasomatism have affected garnet compositions in other sub-cratonic areas of the northern East European Platform (Shchukina et al. 2019) and the Kaapvaal Craton (Gréau et al. 2011), indicating that such metasomatic transformations are not unique to the East Greenland SCLM (Fig. 5).

Garnet in both types of samples (I and II) contains uniformly distributed inclusions (Fig. 3). Their spatial occurrence in garnet (i.e., within whole grain cores and core domains) is not correlated with the contents of mobile elements related to metasomatism. This suggests the inclusions are unrelated and formed prior to metasomatic overprinting.

Higher garnet Zr contents correlate positively with higher garnet Zr/Hf ratios (Fig. 7a), and the same relationship is exhibited by the whole-rock samples (Fig. 7d). As such, the Zr/Hf of the samples were modified during metasomatism from initially low, sub-chondritic values to high, nearly chondritic values (~ 37). Due to the similar geochemical behaviour of Zr and Hf, the source of the metasomatic agent likely had a chondritic Zr/Hf ratio. Therefore, any explanation for the origin of the garnet pyroxenites and eclogite prior to metasomatism has to consider their sub-chondritic Zr/Hf ratios.

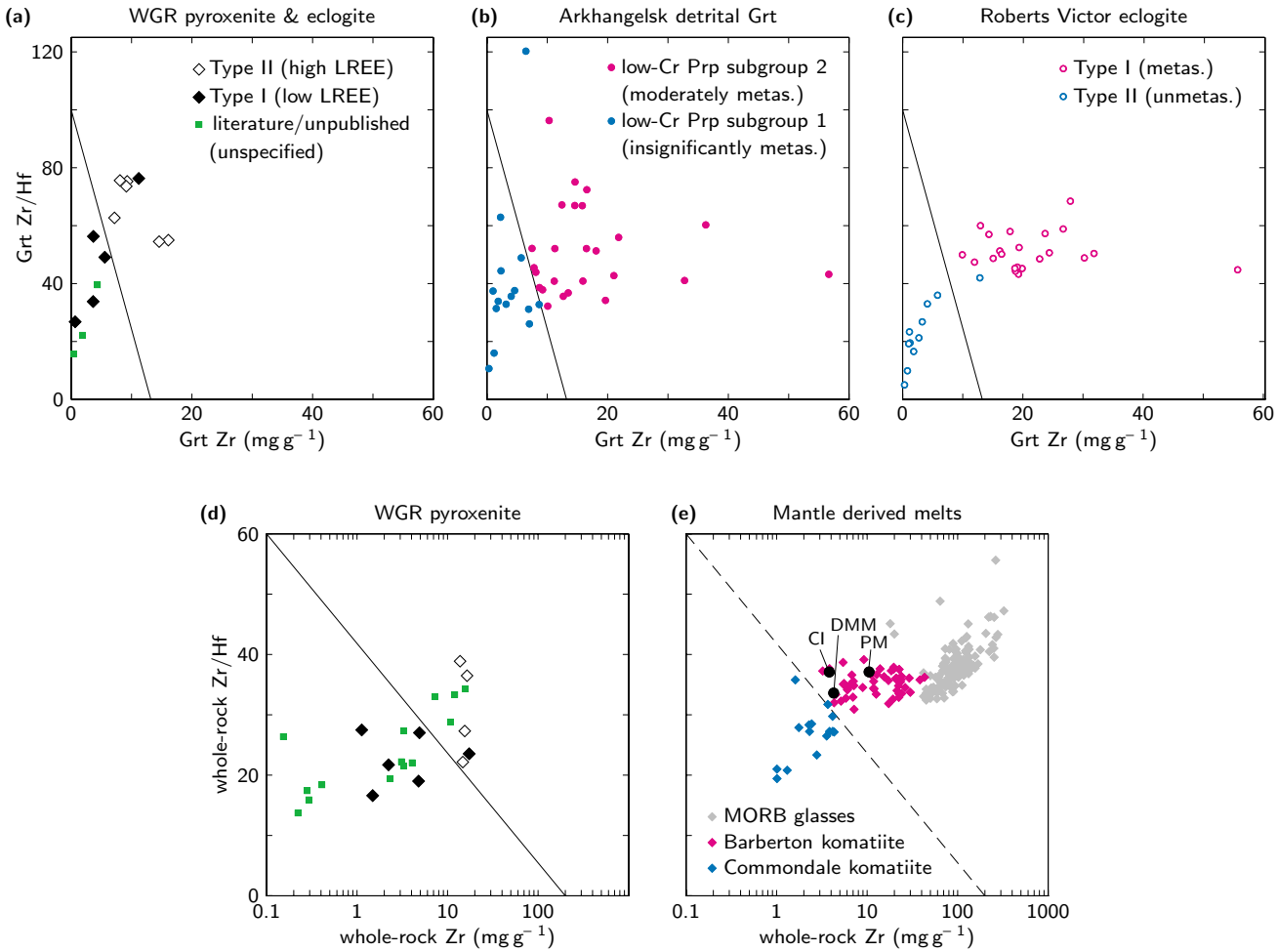

Fig. 7 Plots of Zr/Hf versus Zr for garnet and whole-rock mantle-derived pyroxenites, eclogites, and melts. **a** Western Gneiss Region garnet data from this study (Table SI-3) and the literature (Tables SI-7 and -8). **b** Arkhangelsk detrital garnet (Shchukina et al. 2019). **c** Roberts Victor eclogite garnet (Gréau et al. 2011). **d** Whole-rock data for Western Gneiss Region pyroxenites from this study (Table SI-5) and the literature (Table SI-8). **e** Whole-rock data for MORB glasses (Yang et al. 2018) and different types of South African komatiites (Wilson 2003; Robin-Popieul et al. 2012; Hoffmann and Wilson 2017). The solid line separates compositions related to different degrees of metasomatic enrichment, with the exception of a single data point. The dashed line separates compositions of high-pressure melts from different mantle sources. CI chondrite and PM are values from McDonough and Sun (1995), and the depleted MORB mantle (DMM) composition is from Workman and Hart (2005)

Zirconium and Zr/Hf constraints on the origins of the studied samples

The incompatible behaviour of Zr during mantle melting is evident from the Zr enrichment by one to two orders of magnitude in mid-ocean ridge basalts (MORBs) compared with depleted MORB mantle (Fig. 7e). MORB glasses with high Zr contents have super-chondritic Zr/Hf ratios (Fig. 7e; Yang et al. 2018). This correlation has been suggested to reflect the higher incompatibility of Zr relative to Hf (Niu 2012). Conversely, this means that a melt residue should develop sub-chondritic Zr/Hf ratios with decreasing Zr contents, which is consistent with the model compositions for primitive and depleted MORB mantle (Fig. 7e). This sub-chondritic Zr/Hf ratio may then be inherited in subsequent melts derived from the depleted residues.

Mantle melting during the Archaean is known to have formed—in addition to other magmas—different types of komatiites that reflect different degrees and sequences of upper mantle melt extraction and fractionation (Nesbitt et al. 1979; Robin-Popieul et al. 2012). These processes are reflected by the compositions of Al-depleted, Al-undepleted, and Al-enriched komatiites from the Barberton Greenstone Belt (Fig. 7e). Their super-chondritic Zr contents are approximately one order of magnitude lower than those of modern MORB glasses, but variations in Zr/Hf ratios are minor, which may suggest the Barberton komatiites and many modern MORBs had similar source compositions. In contrast, Archaean mantle-derived melts with sub-chondritic Zr contents, like the Commondale komatiites, exhibit a positive correlation between Zr and Zr/Hf values. Such melts are thought to have had a strongly melt-depleted garnet-bearing source (Hoffmann and Wilson 2017).

The WGR type I garnet pyroxenites and Commondale komatiites share the following characteristics: sub-chondritic Zr contents, sub-chondritic Zr/Hf ratios, positive correlations between Zr and Zr/Hf, and an Al-rich composition (Fig. 7d–e; Table SI-2; Wilson 2003). This supports the interpretation that the WGR sample suite formed by melting of a garnet-bearing, melt-depleted mantle source. A similar hypothesis was proposed based on the whole-rock chemistry of other WGR garnet pyroxenites (Spengler et al. 2018).

If anhydrous melting occurred, then the source rocks of the WGR garnet pyroxenites underwent melting in the presence of a thermal anomaly. Such a mantle plume would have involved whole-mantle convection, which is thought to have been able to transport Archaean oceanic crust during its descent into the stability field of garnet and pyroxene, majorite garnet (Irifune et al. 1986) and then into that of $(Mg,Fe)SiO_3$ and $CaSiO_3$ perovskite minerals (Irifune et al. 1996; Akaogi 2007). Its ascent would then have caused these multiple mineral conversions to occur in the opposite direction. During the passage from the lower to the upper mantle, the recycled components would have either transformed from perovskite minerals back to eclogite minerals, which subsequently would have melted earlier than the host peridotite (Sobolev et al. 2005). Alternatively, the rising recycled oceanic crust and the peridotite could have formed a 'marble-cake' mantle (Allègre and Turcotte 1986), which would have melted as a whole if the lithological composite has had enough time for chemical equilibration. In either case, mantle melting in a plume (Herzberg and Zhang 1996; Robin-Popieul et al. 2012) would have started far beyond the equilibration depth of the WGR garnet pyroxenites (corresponding to 3.4 ± 0.4 GPa; Spengler et al. 2021) and would have allowed for pressures and temperatures required for majorite garnet to crystallise (Gasparik 2014).

Alternatively, if hydrous melting occurred, then the release of water (i.e., by dehydration of hydrous minerals in a subducting plate) would have lowered the solidus of overlying peridotite. This water release would have occurred at depth below the crystallisation depths of the WGR garnet pyroxenites (i.e., at pressures $> 3.4 \pm 0.4$ GPa). In this case, lowering of the solidus counteracts the pressure and temperature dependent stability of the super-silicic component in garnet, which occurs for a given pressure of 3.4 GPa at 1600 °C (Gasparik 2014). Such high temperatures are unusual for mantle wedges (Gerya et al. 2002; Warren et al. 2008) and meet the 0 $\mu g\, g^{-1}$ H_2O peridotite solidus (Sarafian et al. 2017) in contradiction to hydrous conditions of melting. In addition, current experimental and thermodynamic datasets do not suggest majoritic garnet is stable at subduction zone temperatures at $\sim$ 100 km depth. Therefore, hydrous melting is unlikely to explain the formation of the WGR garnet pyroxenites, which contain majoritic garnet precursors.

The general rarity of sub-chondritic Zr/Hf ratios in rocks that formed from mantle melts and have overlapping crystallisation ages (WGR garnet pyroxenites $= 3.33 \pm 0.19$ Ga; Spengler et al. 2009; Commondale komatiites $= 3.334 \pm 0.018$ Ga; Wilson and Carlson 1989; 3.333 ± 0.019 Ga; Hoffmann and Wilson 2017) suggest that the East Greenland and Kaapvaal cratons had a similar palaeogeographic location in the mid-Archaean.

Conclusions

A mineral and whole-rock geochemical study of 10 garnet pyroxenites and 1 eclogite from the East Greenland SCLM exposed in orogenic peridotite bodies across the WGR leads to the following conclusions:

(1) Limited whole-rock middle–heavy REE fractionation and compositional variations suggest the samples had a common origin.
(2) Light REE, Sr, Th, and Zr contents and Zr/Hf ratios subdivide the sample suite into two types. High values (type II samples) are interpreted to record metasomatism that overprinted initially low values (type I samples).
(3) Sub-chondritic Zr contents and Zr/Hf ratios of the type I samples are positively correlated. Low values are indicative of an origin related to a melt-depleted Al-bearing source.
(4) Low Zr/Hf ratios and majorite garnet crystallisation require deep melting associated with a thermal anomaly and recycled oceanic crust.

Supplementary Information The online version contains supplementary material available at https://doi.org/10.1007/s00410-023-02038-4.

Acknowledgements The Institute of Geosciences in the University of Potsdam is thanked for supporting the BSc students Thomas Schirmer and Sebastian Gütte who processed most of the whole-rock samples used in this study. Thomas Theye is thanked for analytical support at the IMK.

Funding This research was not supported by any specific grant from funding agencies in the public, commercial, or not-for-profit sectors. The preparation of this manuscript benefited from financial support of the Norwegian Financial Mechanism 2014–2021 (project 2020/37/K/ST10/02784) granted to DS.

Data availability All data derived from this research are presented in the enclosed figures and supplemented tables.

References

Akaogi M (2007) Phase transitions of minerals in the transition zone and upper part of the lower mantle. Geol Soc Am Spec Pap 421:1–13
Allègre CJ, Turcotte DL (1986) Implications of a two-component marble-cake mantle. Nature 323:123–127
Beyer EE, Brueckner HK, Griffin WL, O'Reilly SY, Graham S (2004) Archean mantle fragments in Proterozoic crust, Western Gneiss Region, Norway. Geology 32:609–612
Beyer EE, Griffin WL, O'Reilly SY (2006) Transformation of Archaean lithospheric mantle by refertilization: evidence from exposed peridotites in the Western Gneiss Region, Norway. J Petrol 47:1611–1636
Beyer EE, Brueckner HK, Griffin WL, O'Reilly SY (2012) Laurentian provenance of Archean mantle fragments in the Proterozoic Baltic crust of the Norwegian Caledonides. J Petrol 53:1357–1383
Brueckner HK (1998) Sinking intrusion model for the emplacement of garnet-bearing peridotites into continent collision orogens. Geology 26:631–634
Brueckner HK (2018) The great eclogite debate of the Western Gneiss Region, Norwegian Caledonides: the in situ crustal v. exotic mantle origin controversy. J Metamorph Geol 36:517–527
Brueckner HK, Carswell DA, Griffin WL (2002) Paleozoic diamonds within a Precambrian peridotite lens in UHP gneisses of the Norwegian Caledonides. Earth Planet Sci Lett 203:805–816
Brueckner HK, Carswell DA, Griffin WL, Medaris LG Jr, van Roermund HLM, Cuthbert SJ (2010) The mantle and crustal evolution of two garnet peridotite suites from the Western Gneiss Region, Norwegian Caledonides: an isotopic investigation. Lithos 117:1–19
Carswell DA (1973) Garnet pyroxenite lens within Ugelvik layered garnet peridotite. Earth Planet Sci Lett 20:347–352
Carswell DA, Harvey MA, Al-Samman A (1983) The petrogenesis of contrasting Fe-Ti and Mg-Cr garnet peridotite types in the high grade gneiss complex of Western Norway. Bull Minéral 106:727–750
Cocks LRM, Torsvik TH (2005) Baltica from the late Precambrian to mid-Palaeozoic times: the gain and loss of a terrane's identity. Earth-Sci Rev 72:39–66
Cuthbert S, van Roermund H (2010) New evidence for majoritic garnet in central-belt orogenic peridotites of the Western Gneiss Complex, Norwegian Caledonides. Geophys Res Abstr 12:EGU2010-14460
Cuthbert SJ, Carswell DA, Krogh-Ravna EJ, Wain A (2000) Eclogites and eclogites in the Western Gneiss Region, Norwegian Caledonides. Lithos 52:165–195
Cutts JA, Smit MA, Spengler D, Kooijman E, van Roermund HLM (2019) Two billion years of mantle evolution in sync with global tectonic cycles. Earth Planet Sci Lett 528:115820
Dobrzhinetskaya LF, Eide EA, Larsen RB, Sturt BA, Trønnes RG, Smith DC, Taylor WR, Posukhova TV (1995) Microdiamond in high-grade metamorphic rocks from the Western Gneiss region, Norway. Geology 23:597–600
Gasparik T (2014) Phase Diagrams for Geoscientists - An Atlas of the Earth's Interior. Springer, New York, p 462
Gee DG, Janák M, Majka J, Robinson P, van Roermund H (2013) Subduction along and within the Baltoscandian margin during closing of the Iapetus Ocean and Baltica- Laurentia collision. Lithosphere 5:169–178
Gerya TV, Stöckhert B, Perchuk AL (2002) Exhumation of high-pressure metamorphic rocks in a subduction channel: a numerical simulation. Tectonics 21:1056
Gieré R (1990) Hydrothermal mobility of Ti, Zr and REE: examples from the Bergell and Adamello contact aureoles (Italy). Terra Nova 2:60–67
Gréau Y, Huang J-X, Griffin WL, Renac C, Alard O, O'Reilly SY (2011) Type I eclogites from Roberts Victor kimberlites: products of extensive mantle metasomatism. Geochim Cosmochim Acta 75:6927–6954
Griffin WL, Råheim A (1973) Convergent metamorphism of eclogites and dolerites, Kristiansund area, Norway. Lithos 6:21–40
Griffin WL, Austrheim H, Brastad K, Bryhni I, Krill AG, Krogh EJ, Mørk MBE, Qvale H, Tørudbakken B (1985) High-pressure metamorphism in the Scandinavian Caledonides. In: Gee DG, Sturt BA (eds) The Caledonide orogen-Scandinavia and related areas. Wiley, Chichester, pp 783–801

Griffin WL, O'Reilly SY, Abe N, Aulbach S, Davies RM, Pearson NJ, Doyle BJ, Kivi K (2003) The origin and evolution of Archean lithospheric mantle. Precambr Res 127:19–41

Herzberg C (2004) Geodynamic information in peridotite petrology. J Petrol 45:2507–2530

Herzberg C, Zhang J (1996) Melting experiments on anhydous peridotite KLB-1: compositions of magmas in the upper mantle and transition zone. J Geophys Res 101:8271–8295

Hoffmann JE, Wilson A (2017) The origin of highly radiogenic Hf isotope compositions in 3.33 Ga Commondale komatiite lavas (South Africa). Chem Geol 455:6–21

Irifune T, Sekine T, Ringwood AE, Hibberson WO (1986) The eclogite-garnetite transformation at high pressure and some geophysical implications. Earth Planet Sci Lett 77:245–256

Irifune T, Koizumi T, Ando J-i (1996) An experimental study of the garnet-perovskite transformation in the system $MgSiO_3$-$Mg_3\ Al_2\ Si_3\ O_{12}$. Phys Earth Planet Inter 96:147–157

Jamtveit B, Carswell DA, Mearns EW (1991) Chronology of the high-pressure metamorphism of Norwegian garnet peridotites/pyroxenites. J Metamorph Geol 9:125–139

John T, Scherer EE, Haase K, Schenk V (2004) Trace element fractionation during fluid-induced eclogitization in a subducting slab: trace element and Lu-Hf-Sm-Nd isotope systematics. Earth Planet Sci Lett 227:441–456

Krabbendam M, Wain A, Andersen TB (2000) Pre-Caledonian granulite and gabbro enclaves in the Western Gneiss Region, Norway: indications of incomplete transition at high pressure. Geol Mag 137:235–255

Kullerud L, Tørudbakken BO, Ilebekk S (1986) A compilation of radiometric age determinations from the Western Gneiss Region, south Norway. Nor geol unders bull 406:17–42

Lapen TJ, Medaris LG Jr, Johnson CM, Beard BL (2005) Archean to Middle Proterozoic evolution of Baltica subcontinental lithosphere: evidence from combined Sm-Nd and Lu-Hf isotope analyses of the Sandvik ultramafic body, Norway. Contrib Mineral Petrol 150:131–145

Massonne H-J, Opitz J, Theye T, Nasir S (2013) Evolution of a very deeply subducted metasediment from As Sifah, northeastern coast of Oman. Lithos 156–159:171–185

McDonough WF, Sun S-s (1995) The composition of the Earth. Chem Geol 120:223–253

Mearns EW (1986) Sm-Nd ages for Norwegian garnet peridotite. Lithos 19:269–278

Nesbitt RW, Sun S-s, Purvis AC (1979) Komatiites: geochemistry and genesis. Can Mineral 17:165–186

Niu Y (2012) Earth processes cause Zr-Hf and Nb-Ta fractionations, but why and how? RSC Adv 2:3587–3591

Pearson DG, Wittig N (2008) Formation of Archaean continental lithosphere and its diamonds: the root of the problem. J Geol Soc 165:895–914

Robin-Popieul CCM, Arndt N, Chauvel C, Byerly GR, Sobolev AV, Wilson A (2012) A new model for Barberton komatiites: deep critical melting with high melt retention. J Petrol 53:2191–2229

Sarafian E, Gaetani GA, Hauri EH, Sarafian AR (2017) Experimental constraints on the damp peridotite solidus and oceanic mantle potential temperature. Science 355:942–945

Seljebotn JV (2016) Structural and petrological survey of peridotite at Almklovdalen, Norway. MSc thesis, University of Bergen

Shchukina EV, Agashev AM, Shchukin VS (2019) Diamond-bearing root beneath the northern East European Platform (Arkhangelsk region, Russia): evidence from Cr-pyrope trace-element geochemistry. Minerals 9:261

Smith DC, Godard G (2013) A Raman spectroscopic study of diamond and disordered sp^3-carbon in the coesite-bearing Straumen Eclogite Pod, Norway. J Metamorph Geol 31:19–33

Sobolev AV, Hofmann AW, Sobolev SV, Nikogosian IK (2005) An olivine-free mantle source of Hawaiian shield basalts. Nature 434:590–597

Spengler D (2006) Origin and evolution of deep upper mantle rocks from western Norway. Dissertation, Universiteit Utrecht

Spengler D, van Roermund HLM, Drury MR, Ottolini L, Mason PRD, Davies GR (2006) Deep origin and hot melting of an Archaean orogenic peridotite massif in Norway. Nature 440:913–917

Spengler D, Brueckner HK, van Roermund HLM, Drury MR, Mason PRD (2009) Long-lived, cold burial of Baltica to 200 km depth. Earth Planet Sci Lett 281:27–35

Spengler D, van Roermund HLM, Drury MR (2018) Deep komatiite signature in cratonic mantle pyroxenite. J Metamorph Geol 36:591–602

Spengler D, van Roermund HLM, Scheffler F (2019) Pyroxene exsolution microstructures in garnet from the Almklovdalen peridotite, SW Norway. Lithos 350–351:105217

Spengler D, Alifirova TA, van Roermund HLM (2021) Subcratonic and tectonic evolution of pyroxenite and eclogite with lamellar inclusions in garnet, Western Gneiss Region, Norway. J Petrol 62:egab008

Steinberger B, Bredow E, Lebedev S, Schaeffer A, Torsvik TH (2019) Widespread volcanism in the Greenland-North Atlantic region explained by the Iceland plume. Nat Geosci 12:61–68

Terry MP, Robinson P, Carswell DA, Gasparik T (1999) Evidence for a Proterozoic mantle plume and a thermotectonic model for exhumation of garnet peridotites, Western Gneiss Region, Norway. EOS Trans Am Geophys Union 80:S359–S360

Tsay A, Zajacz Z, Ulmer P, Sanchez-Valle C (2017) Mobility of major and trace elements in the eclogite-fluid system and element fluxes upon slab dehydration. Geochim Cosmochim Acta 198:70–91

Tucker RD, Krogh TE, Råheim A (1990) Proterozoic evolution and age-province boundaries in the central part of the Western Gneiss Region, Norway: results of U-Pb dating of accessory minerals from Trondheimsfjord to Geiranger. In: Gower CF, Ryan B, Rivers T (eds) Mid-Proterozoic Laurentia-Baltica. Geological Association of Canada, St. John's, pp 149–173

van Roermund HLM, Drury MR (1998) Ultra-high pressure (P > 6 GPa) garnet peridotites in western Norway: exhumation of mantle rocks from > 185 km depth. Terra Nova 10:295–301

Wain A, Waters D, Jephcoat A, Olijynk H (2000) The high-pressure to ultrahigh-pressure eclogite transition in the Western Gneiss Region, Norway. Eur J Mineral 12:667–687

Walter MJ (1998) Melting of garnet peridotite and the origine of komatiite and depleted lithosphere. J Petrol 39:29–60

Warren C, Beaumont C, Jamieson RA (2008) Modelling tectonic styles and ultra-high pressure (UHP) rock exhumation during the transition from oceanic subduction to continental collision. Earth Planet Sci Lett 267:129–145

Wilson AH (2003) A new class of silica enriched, highly depleted komatiites in the southern Kaapvaal Craton, South Africa. Precambr Res 127:125–141

Wilson A, Carlson R (1989) A Sm-Nd and Pb isotope study of Archaean greenstone belts in the southern Kaapvaal Craton, South Africa. Earth Planet Sci Lett 96:89–105

Workman RK, Hart SR (2005) Major and trace element composition of the depleted MORB mantle (DMM). Earth Planet Sci Lett 231:53–72

Yang S, Humayun M, Salters VJM (2018) Elemental systematics in MORB glasses from the Mid-Atlantic Ridge. Geochem Geophys Geosyst 19:4236–4259